Acta Cryst B
STRUCTURAL SCIENCE
CRYSTAL ENGINEERING
MATERIALS
ISSN 2052-5206

Crystal structures of zinc(II) complexes with β-hydroxypyridinecarboxylate ligands: examples of structure-directing effects used in inorganic crystal engineering

Nóra Veronika May,[a]* Kevin Nys,[b] H. Y. Vincent Ching,[b] Laura Bereczki,[a,c] Tamás Holczbauer,[a,d] Valerio B. Di Marco[e] and Petra Bombicz[a]

[a]Centre for Structural Sciences, Research Centre for Natural Sciences, Magyar tudósok körútja 2, Budapest, H-1117, Hungary, [b]Department of Chemistry, University of Antwerp, Universiteitsplein 1, Antwerpen, B-2610, Belgium, [c]Institute of Materials and Environmental Chemistry, Research Centre for Natural Sciences, Magyar tudósok körútja 2, Budapest, H-1117, Hungary, [d]Institute of Organic Chemistry, Research Centre for Natural Sciences, Magyar tudósok körútja 2, Budapest, H-1117, Hungary, and [e]Department of Chemical Sciences, University of Padova, via Marzolo 1, Padova, 35131, Italy. *Correspondence e-mail: may.nora@ttk.hu

Received 27 October 2020
Accepted 9 January 2021

Edited by J. Lipkowski, Polish Academy of Sciences, Poland

Keywords: zinc(II) complex; hydroxypyridinecarboxylic acid; inorganic crystal engineering; trigonal bipyramidal geometry; tau value; CSD; coordination geometry.

CCDC references: 2009100; 2009101; 2009102; 2009103

Supporting information: this article has supporting information at journals.iucr.org/b

The coordination properties of four hydroxypyridinecarboxylates, designed for the treatment of iron-overloading conditions as bidentate *O*,*O*′-donor ligands, have been studied with Zn^{II} in the solid state. The coordination compounds $[Zn(A1)_2(H_2O)_2]$ (**1**), $[Zn(A2)_2(H_2O)]$ (**2**), $[Zn(A3)_2(H_2O)]\cdot 2H_2O$ (**3**) and $[Zn_2(B1)_4(H_2O)_2]\cdot 4H_2O$ (**4**), where the ligands are 1-methyl-4-oxidopyridinium-3-carboxylate (A1, $C_7H_6NO_3$), 1,6-dimethyl-4-oxidopyridinium-3-carboxylate (A2, $C_8H_8NO_3$), 1,5-dimethyl-4-oxido-pyridinium-3-carboxylate (A3, $C_8H_8NO_3$) and 1-methyl-3-oxidopyridinium-4-carboxylate (B1, $C_7H_6NO_3$), have been synthesized and analysed by single-crystal X-ray diffraction. The ligands were chosen to probe (i) the electronic effects of inverting the positions of the O-atom donor groups (*i.e.* A1 *versus* B1) and (ii) the electronic and steric effects of the addition of a second methyl group in different positions on the pyridine ring. Two axially coordinated water molecules resulting in a six-coordinated symmetrical octahedron complement the bis-ligand complex of A1. Ligands A2 and A3 form five-coordinated trigonal bipyramidal complexes with one additional water molecule in the coordination sphere, which is a rarely reported geometry for Zn^{II} complexes. Ligand B1 shows a dimeric structure, where the two Zn^{2+} dications have slightly distorted octahedral geometry and the pyridinolate O atom of the neighbouring complex bridges them. The coordination spheres of the Zn^{2+} dications and the supramolecular structures are discussed in detail. The packing arrangements of **1**–**3** are similar, having alternating hydrophilic and hydrophobic layers, however the similarity is broken in **4**. The obtained coordination geometries are compared with their previously determined Cu^{II} analogues. The study of the individual complexes is complemented with a comprehensive analysis of Zn^{II} complexes with oxygen donor ligands with data from the Cambridge Structural Database.

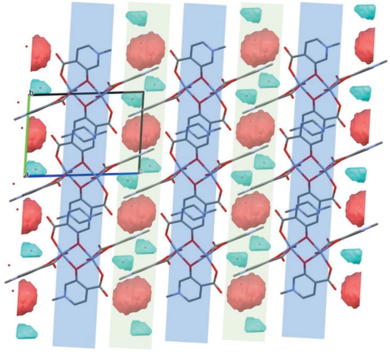

1. Introduction

Hydroxypyridinecarboxylic acid (HPC) derivatives have been considered (Di Marco *et al.*, 2002; Crisponi *et al.*, 2013; Sija *et al.*, 2014; Dean *et al.*, 2018) as potential chelating agents for the treatment of iron-overloading conditions. The design of these compounds was based on deferiprone (1,2-dimethyl-3-hydroxypyridin-4-one), which is a globally used iron-chelating drug. *In vitro* studies have shown that Cu^{II} and Zn^{II} are the

most competitive metal ions against Fe^{III} and are able to considerably affect the formation of Fe^{III} complexes of these iron chelators (Clarke & Martell, 1992; Pashadilis & Kontoghiorghes, 2001; Li, 2019). Investigating the complexation of HPCs to Cu^{II} and Zn^{II} is of importance as the displacement of these essential metal ions by chelating drugs could adversely affect the biological processes dependent on these metals, potentially causing toxicity. The complexation properties of several HPCs towards Cu^{II} in the solid and solution states have been reported recently (May *et al.*, 2019), showing the influence of electron distribution on the coordination properties of Cu^{II} with HPCs of different methyl, hydroxyethyl and carboxyethyl derivatives. While all HPC ligands were found to coordinate Cu^{II} through the deprotonated O-atom donors (oxide and carboxylate), their arrangement in $[CuL_2]$ resulted in distinct structures. Solution equilibrium studies and density functional theory (DFT) calculations revealed a significant difference in the electronegativity of the donor carboxylate and hydroxy O atoms. A correlation between the increasing acidity of the OH group with complex stability was observed. These electronic differences can also be used to rationalize the formation of bridging dimers, as well as of *cis* or *trans* arrangements. Solution speciation of ligand A3 (DQ715, 1,5-dimethyl-4-oxidopyridinium-3-carboxylate) with Cu^{II} and Zn^{II} has been reported previously (Sija *et al.*, 2014) and it was found that A3 forms only mononuclear complexes with Zn^{II}, *i.e.* $[ZnL]$ and $[ZnL_2]$, and the stabilities of the formed complexes are lower compared to their Cu^{II} analogues. With these divalent metal ions the stability of the obtained complex is significantly lower than the stability with Fe^{III} or Al^{III}, which makes HPCs good candidates as Fe^{III} or Al^{III} chelators.

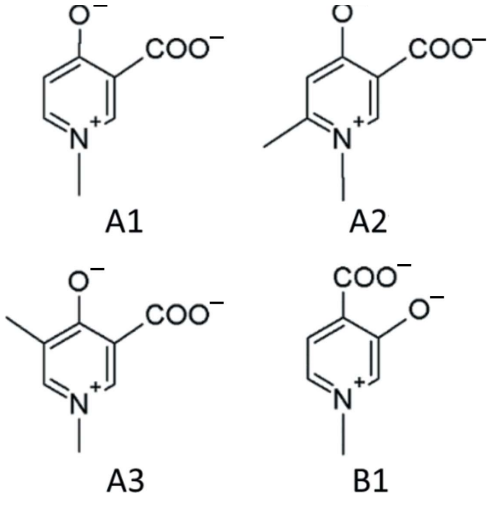

Figure 1
The structures of the investigated ligands in their fully deprotonated ionic forms. From now on, the compounds in this article will be referred to with the names A1–A3 and B1, omitting the charge for the sake of simplicity. In the literature relating to these compounds, the following acronyms have been used for A1–A3 and B1, respectively: DQ1, DQ716, DQ715 and DT1 (Crisponi *et al.*, 2013).

Following on from this previous work, we report here our solid-state studies on the complexation to Zn^{II} of four HPC ligands, namely, 1-methyl-4-oxidopyridinium-3-carboxylate (A1), 1,6-dimethyl-4-oxidopyridinium-3-carboxylate (A2), 1,5-dimethyl-4-oxido-pyridinium-3-carboxylate (A3) and 1-methyl-3-oxidopyridinium-4-carboxylate (B1) (Fig. 1), by single-crystal X-ray diffraction. The ligands were selected to investigate the different effects on complexation of (i) the inductive effects when the positions of the O-atom donor groups are inverted (*i.e.* A1 *versus* B1) and (ii) the electronic and steric effects of the addition of a second methyl group in different positions on the pyridine ring (*i.e.* A1 *versus* A2 *versus* A3). We have also compared the structures of the Zn^{II} complexes of A1–A3 and B1 with other previously reported O-atom-donor ligand-containing Zn^{II} complexes. A comprehensive coordination geometry analysis by data mining using the Cambridge Structural Database (CSD, Version 2020.1; Groom *et al.*, 2016) was performed. When available, the Zn^{II} complex structures of A1–A3 and B1 were also compared with their Cu^{II} analogues (Figs. S1–S3 in the supporting information) because although Cu^{II} and Zn^{II} can form complexes with the same ligands, the geometries of the resulting complexes are usually different owing to their different electronic configurations. As Cu^{II} has a d^9 electronic configuration, the most common geometries are elongated octahedral or square pyramidal, as a consequence of the Jahn–Teller effect, while in the case of Zn^{II}, the d^{10} electronic configuration prefers the very symmetrical tetragonal and octahedral geometries.

Our structural comparison of Cu^{II} and Zn^{II} complexes containing the same and related ligands also revealed the structural features originating from (i) the steric and electronic effects of the ligands themselves, (ii) the geometrical preferences of the metal ions and (iii) the intermolecular forces between the molecules in the crystals. These are important aspects of the goals of inorganic crystal engineering (ICE), where coordination bonds connect metal ions and organic building blocks to each other. ICE aims at a better understanding of structure-directing effects in order to find strategies to control molecular self-assembly (Biradha *et al.*, 2011; Desiraju, 2003).

2. Experimental

2.1. Chemicals and crystallization

HPCs were synthesized as described previously (Di Marco *et al.*, 2006; Dean *et al.*, 2009, 2014). The Zn^{II} stock solution was prepared from $ZnCl_2$ (Sigma–Aldrich) dissolved in doubly distilled water. The concentration was checked by ICP–OES. The NaOH, HCl and buffer solutions used in the pH adjustment were purchased from Sigma–Aldrich. Typically, the ligand (2 mg) was dissolved in water (2 ml) and $ZnCl_2$ solution was added to obtain a twofold ligand excess. The pH was adjusted with NaOH to 7.0. After about 2–3 weeks, colourless single crystals appeared. Single crystals suitable for X-ray diffraction were obtained by slow evaporation from aqueous solution. A crystal was selected for

Table 1
Experimental details.

	1	**2**	**3**	**4**
Crystal data				
Chemical formula	$[Zn(C_7H_6NO_3)_2(H_2O)_2]$	$[Zn(C_8H_8NO_3)_2(H_2O)]$	$[Zn(C_8H_8NO_3)_2(H_2O)]\cdot 2H_2O$	$[Zn_2(C_7H_6NO_3)_4(H_2O)_2]\cdot 4H_2O$
M_r	405.66	415.71	451.72	847.35
Crystal system, space group	Triclinic, $P\overline{1}$	Triclinic, $P\overline{1}$	Monoclinic, $C2/c$	Triclinic, $P\overline{1}$
Temperature (K)	293	138	103	103
a, b, c (Å)	7.2924 (5), 7.4450 (5), 8.0936 (6)	8.2959 (3), 10.1989 (4), 10.3466 (4)	10.8962 (4), 10.3334 (3), 16.6916 (7)	7.9237 (5), 8.5740 (5), 12.3954 (8)
α, β, γ (°)	97.966 (7), 103.385 (7), 115.659 (5)	70.187 (5), 82.585 (6), 79.659 (6)	90, 108.435 (1), 90	84.248 (2), 74.706 (2), 85.908 (2)
V (Å^3)	370.76 (5)	808.01 (6)	1782.94 (11)	807.32 (9)
Z	1	2	4	1
Radiation type	Cu $K\alpha$	Cu $K\alpha$	Mo $K\alpha$	Mo $K\alpha$
μ (mm^{-1})	2.79	2.53	1.43	1.58
Crystal size (mm)	0.45 × 0.40 × 0.30	0.50 × 0.20 × 0.10	0.50 × 0.50 × 0.30	0.50 × 0.20 × 0.20
Data collection				
Diffractometer	Rigaku R-AXIS RAPID	Rigaku R-AXIS RAPID	Rigaku R-AXIS RAPID	Rigaku R-AXIS RAPID
Absorption correction	Numerical (*NUMABS*; Higashi, 2011)	Numerical (*NUMABS*; Higashi, 2011)	Numerical (*NUMABS*; Higashi, 2002)	Numerical (*NUMABS*; Higashi, 2002)
T_{min}, T_{max}	0.682, 0.828	0.637, 0.894	0.396, 0.765	0.429, 0.777
No. of measured, independent and observed $[I > 2\sigma(I)]$ reflections	5106, 1225, 1209	11 343, 2856, 2715	35 961, 2046, 2020	27 896, 3680, 3521
R_{int}	0.029	0.045	0.046	0.035
$(\sin\theta/\lambda)_{max}$ (Å^{-1})	0.602	0.602	0.649	0.649
Refinement				
$R[F^2 > 2\sigma(F^2)]$, $wR(F^2)$, S	0.029, 0.075, 1.16	0.034, 0.088, 1.07	0.028, 0.075, 1.19	0.024, 0.063, 1.10
No. of reflections	1225	2856	2046	3680
No. of parameters	116	247	142	263
No. of restraints	0	0	0	6
H-atom treatment	H-atom parameters constrained	H atoms treated by a mixture of independent and constrained refinement	H atoms treated by a mixture of independent and constrained refinement	H atoms treated by a mixture of independent and constrained refinement
$\Delta\rho_{max}$, $\Delta\rho_{min}$ (e Å^{-3})	0.34, −0.20	0.53, −0.36	0.58, −0.37	0.50, −0.33

Computer programs: *RAPID-AUTO* (Rigaku, 2015) for **1** and **2**, *CrystalClear* (Rigaku/MSC, 2008) for **3** and **4**, *SIR2014* (Burla *et al.*, 2015), *SHELXT* (Sheldrick, 2015*a*), *SHELXL2014* (Sheldrick, 2015*b*), *Mercury* (Macrae *et al.*, 2020), *PLATON* (Spek, 2020), *WinGX* (Farrugia, 2012) and *publCIF* (Westrip, 2010).

the diffraction experiment from among the several crystals which were left in the saturated solution in order to preserve their quality (yields were *ca* 50%).

2.2. X-ray data collection, structure solution and refinement of compounds 1–4

Crystal data, data collection and structure refinement details for **1**–**4** are summarized in Table 1. H atoms were placed in geometric positions and were included in structure-factor calculations. In general, C-bound H atoms were geometrically located and refined as riding (assuming distances of C—H = 0.96 Å for methyl and C—H = 0.93 Å for aromatic protons, and were refined by $U_{iso} = 1.5U_{eq}$ for methyl and $U_{iso} = 1.2U_{eq}$ for aromatic carrier atoms. The water H atoms were located from difference Fourier maps and then the positions of H_2O were refined as rigid units. Selected bond lengths and angles were calculated using *PLATON* software (Spek, 2020). The calculated powder X-ray diffraction (PXRD) patterns were generated from the single-crystal X-ray diffraction data using *PLATON* (see Figs. S4–S7 in the supporting information).

2.3. Hirshfeld surface analysis

The Hirshfeld surfaces of the investigated molecules in the crystals of **1**–**4** were calculated by *CrystalExplorer* (Turner *et al.*, 2017; Spackman & Jayatilaka, 2009; Spackman & McKinnon, 2002; McKinnon *et al.*, 2004). High-resolution Hirshfeld surfaces were mapped with the functions d_{norm} (normalized contact distance). The Hirshfeld surface of a molecule is generated by points where the contribution to the electron density from the molecule of interest is equal to the contribution from all neighbouring molecules. Each point of this surface has two distances: d_e is the distance from the point to the nearest nucleus external to the surface and d_i the distance to the nearest nucleus internal to the surface. The combination of d_e and d_i in the form of a two-dimensional (2D) fingerprint plot results in unique properties for each crystal and provides a useful tool to compare the intermolecular contacts in the different crystals. Distances involving H atoms were normalized in all calculations of the Hirshfeld surfaces (the C—H and O—H distances were 1.083 and 0.983 Å, respectively). The atomic distances given in the tables and figures throughout this article were calculated based on the single-crystal X-ray diffraction measurements.

3. Results and discussions

3.1. Proton dissociation processes of the ligands

The deprotonation steps of the ligands (AH_2^+) have been determined previously and it was found that the first proton dissociation at very low pH ($pK_{a1} < 1$) can be assigned to the –COOH group. In the neutral AH forms, the –OH proton is involved in an intramolecular hydrogen bond with the deprotonated $–COO^-$ group (Fig. S8 in the supporting information). The fully deprotonated A^- form can be obtained by the second deprotonation at the –OH group which is therefore accompanied by the cleavage of this internal hydrogen bond. The pK_{a2} values are influenced by the inductive effect of the positively charged $>N^+—Me$ groups and the other ring substituents. Another influencing factor is keto–enol tautomerization, which is more likely to occur for 4-hydroxypyridine-3-carboxylates (A1–A3) than for 3-hydroxypyridine-4-carboxylates (B1) (Fig. S8). The previously determined pK_{a2} values resulted in the deprotonation order A1 [5.9578 (6)] < A2 [6.295 (1)] < B1 [6.6326 (8)] < A3 [6.64 (1)] (Di Marco *et al.*, 2009; Dean *et al.*, 2009; Sija *et al.*, 2014; Crisponi *et al.*, 2013).

3.2. Structural analysis of $[Zn(A1)_2(H_2O)_2]$ (1)

The single-crystal X-ray diffraction (SXRD) study showed that $[Zn(A1)_2(H_2O)_2]$ (**1**) crystallizes in the triclinic space group $P\overline{1}$. The asymmetric unit consists of half of the complex (half a metal ion, one anionic A1 ligand and one axially coordinated water molecule), as the Zn1 ion is positioned on an inversion centre (Fig. 2). Zn1 is six-coordinated, exhibiting a distorted octahedral geometry. The pyridine-ring plane

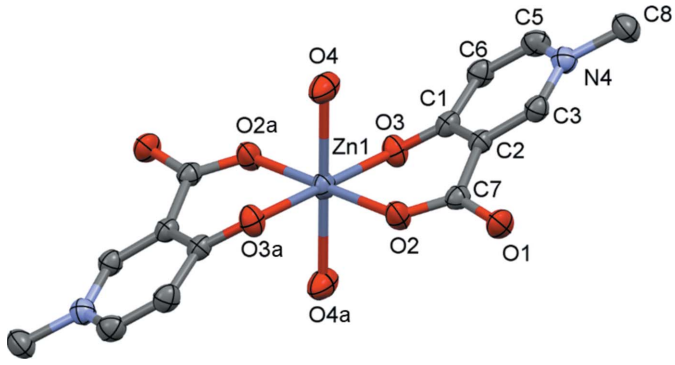

Figure 2
The molecular structure of $[Zn(A1)_2(H_2O)_2]$, **1**, with displacement ellipsoids drawn at the 50% probability level. H atoms have been omitted for clarity. For atom labels. suffix a = $1 - x, -y, 2 - z$.

deviates significantly from the coordination plane, as the dihedral angle between the planes generated by the coordinating atoms O2/Zn1/O3 and the pyridine ring is 23.59 (5)° (Table S1 in the supporting information), while the pyridine-ring planes are parallel owing to the centrosymmetrical arrangement. The obtained Zn—O distances in the coordination sphere agree with the usual distance of 2.1 ± 0.1 Å obtained from the CSD for the Zn—O bond length (Table 2). The two ligands coordinate to the metal ion in a *trans* arrangement (their carboxylate groups are in opposite positions with respect to the equatorial plane). This *trans* coordination geometry of the ligands was found previously in the corresponding Cu^{II} complex. Ligand A1 coordinates to Cu^{II}

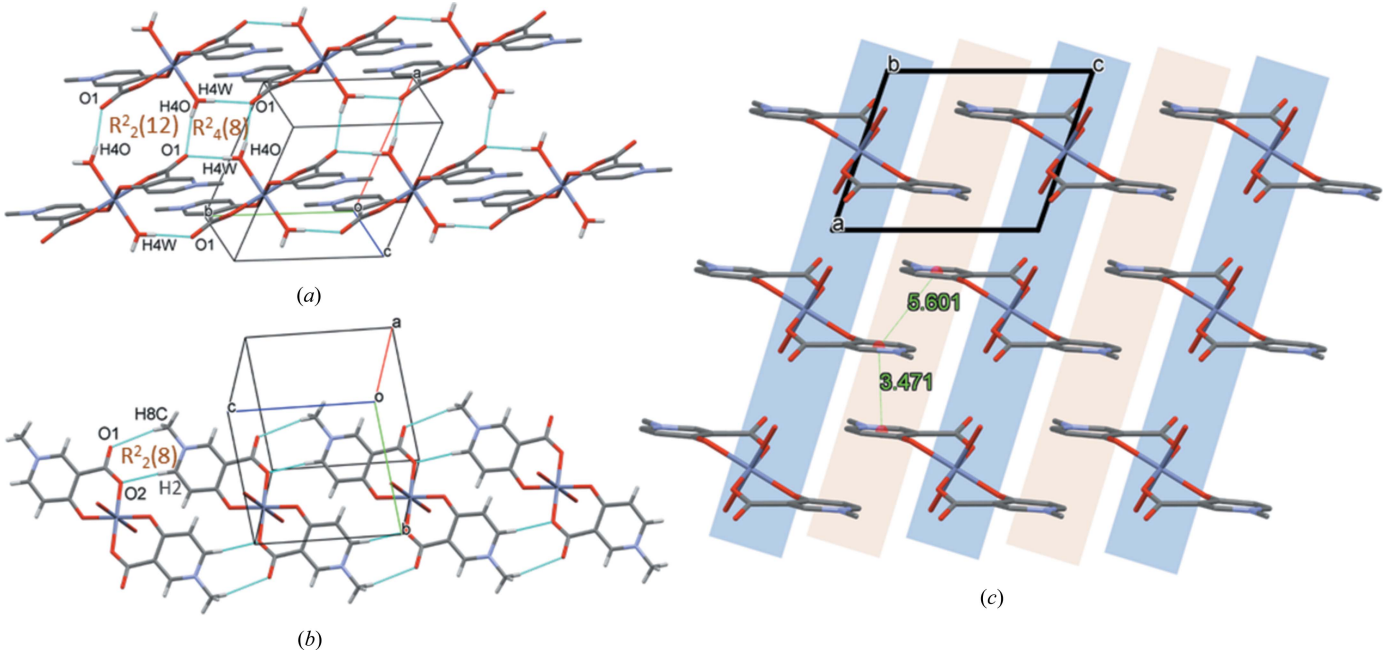

Figure 3
Packing arrangements in **1**, showing the main (*a*) O—H···O and (*b*) C—H···O intermolecular interactions, and (*c*) the alternating hydrophilic (blue) and hydrophobic (grey) layers, viewed from the crystallographic *b* direction. Ring–ring; distances shown in (*c*) are in Å.

Table 2
Selected interatomic distances (Å) and angles (°) in **1**–**4**.

	1	**2**	**3**	**4**
Zn1—O2	2.0249 (15)	1.9619 (17)	2.0282 (12)	2.1198 (12)
Zn1—O3	2.0701 (15)	2.0799 (17)	1.9993 (10)	1.9998 (11)
Zn1—O12	–	1.9729 (17)	–	2.0302 (12)
Zn1—O13	–	2.0454 (17)	–	2.0563 (11)
Zn1—O13a^{i}	–	–	–	2.1613 (11)
Zn1—O4$_{ax}$	2.1794 (19)	2.0042 (18)	2.0046 (19)	2.1478 (12)
O2—Zn1—O3	88.05 (6)	88.70 (7)	88.05 (4)	89.59 (4)
O2—Zn1—O2	180	–	173.31 (7)	–
O3 —Zn1—O3	180	–	137.80 (6)	–
O2—Zn1—O4$_{ax}$	89.61 (7)	123.57 (8)	93.34 (3)	169.23 (5)
O3 —Zn1—O4$_{ax}$	87.39 (7)	88.70 (7)	111.10 (3)	96.94 (5)
O2—Zn1—O12	–	113.47 (7)	–	–
O3—Zn1—O13	–	173.82 (7)	–	175.22 (5)
O12—Zn—O13	–	89.62 (7)	–	169.34 (4)

Symmetry code: (i) $-x, 2-y, 1-z$.

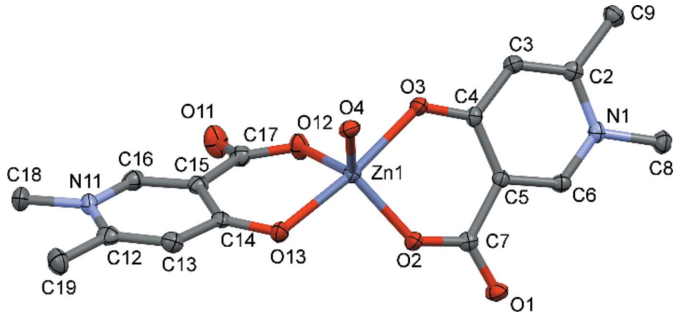

Figure 4
The molecular structure of $[Zn(A2)_2(H_2O)]$, **2**, with displacement ellipsoids drawn at the 50% probability level. H atoms have been omitted for clarity.

with the two ligands in a *trans* arrangement, $[Cu_2(A1)_4]\cdot 4H_2O$, and the noncoordinated carboxylate O atom binds to a neighbouring Cu^{II} centre forming a *syn–anti* carboxylate bridge in an equatorial–axial coordination mode, resulting in a cyclic dimer structure (Fig. S1 in the supporting information; May *et al.*, 2019). The geometry of the Zn^{II} complex of A1 is close to octahedral, while that of Cu^{II} is square pyramidal (Fig. S1 in the supporting information). The equatorial Cu—O2 and Cu—O3 bond lengths were found to be significantly shorter [1.931 (3) and 1.924 (3) Å, respectively] than the axial bond [2.614 (3) Å] in the crystal. In contrast, for **1**, the equatorial Zn—O2 and Zn—O3 distances [2.0249 (15) and 2.0701 (15) Å, respectively] are much closer to that of the axial Zn—O4 bond distance [2.1794 (19) Å]. The distances and angles measured between the atoms of the coordination sphere in the corresponding Zn^{II} and Cu^{II} complexes are collected in Table 2 and Table S2 in the supporting information. The packing arrangements of all measured crystals, viewed from the three crystallographic directions, are collected in Fig. S9 in the supporting information.

In **1**, the main secondary interaction is between the axially coordinated water H atoms and the carboxylate O atom of an adjacent molecule (O4—H4O···O1^{i}). It is repeated by the symmetry centres; thus, two hydrogen-bonded rings are formed, depicted as graph sets $R_4^2(8)$ and $R_2^2(12)$, respectively

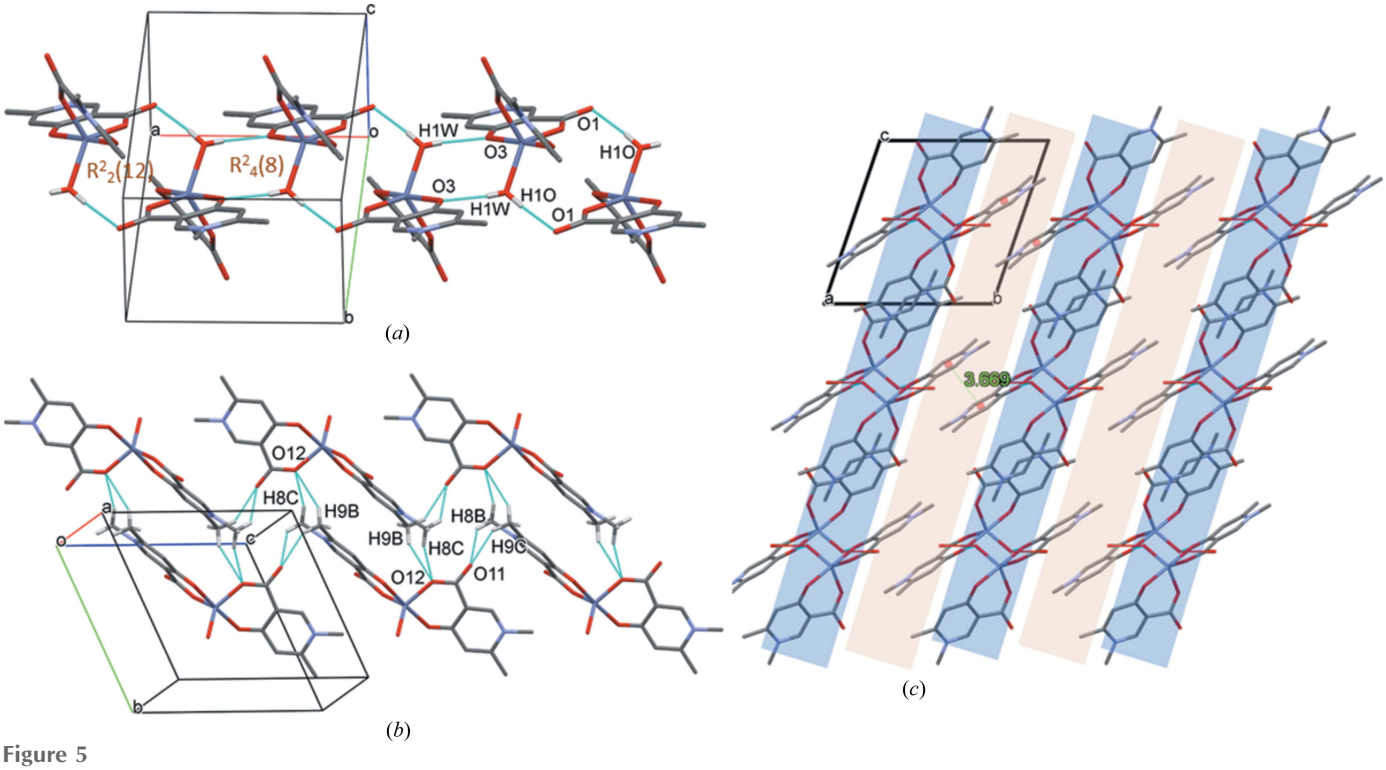

Figure 5
The packing arrangements in **2**, showing the main (*a*) O—H···O and (*b*) C—H···O intermolecular interactions, and (*c*) the alternating hydrophilic (blue) and hydrophobic (grey) layers, viewed from the crystallographic *a* direction. The ring–ring; distance shown in (*c*) is in Å.

Table 3
Hydrogen-bond geometry (Å, °) for **1**–**4**.

D—H···A	D—H	H···A	D···A	D—H···A
Crystal **1**				
O4—H4O···O1^{i}	0.82	2.01	2.814 (3)	167
O4—H4*W*···O1^{ii}	0.84	1.92	2.752 (3)	174
C2—H2···O2^{iii}	0.93	2.34	3.205 (3)	155
C8—H8*C*···O1^{iii}	0.96	2.66	3.354 (3)	129
Crystal **2**				
O4—H1O···O1^{iv}	0.84 (4)	1.87 (4)	2.708 (3)	175 (4)
O4—H1*W*···O3^{v}	0.74 (3)	1.93 (3)	2.668 (2)	174 (4)
C8—H8*B*···O11^{vi}	0.96	2.55	3.296 (4)	135
C8—H8*C*···O12^{vii}	0.96	2.37	3.286 (3)	159
C9—H9*B*···O12^{vii}	0.96	2.55	3.434 (4)	152
C9—H9*C*···O11^{vi}	0.96	2.38	3.140 (3)	136
Crystal **3**				
O4—H4*W*···O5^{viii}	0.79 (3)	1.84 (3)	2.626 (2)	175 (3)
O5—H5O···O1^{ix}	0.79 (3)	2.45 (3)	3.139 (2)	147 (3)
O5—H5*W*···O2	0.78 (3)	1.97 (3)	2.745 (2)	173 (3)
C8—H8*B*···O2^{x}	0.98	2.52	3.496 (2)	174
C8—H8*C*···O1^{v}	0.98	2.48	3.330 (2)	145
Crystal **4**				
O4—H4O···O2^{xi}	0.84 (1)	2.00 (1)	2.823 (2)	164 (2)
O4—H4*W*···O1^{xii}	0.83 (2)	1.88 (2)	2.710 (2)	175 (2)
O5—H5O···O11^{xiii}	0.84 (2)	1.93 (2)	2.761 (2)	174 (2)
O5—H5*V*···O6	0.73 (6)	2.04 (6)	2.765 (2)	179 (2)
O5—H5*W*···O5^{xiv}	0.84 (4)	1.86 (4)	2.700 (2)	178 (4)
O6—H6O···O3^{ii}	0.83 (2)	2.03 (2)	2.853 (2)	168 (2)
O6—H6*V*···O6^{xv}	0.81 (5)	1.95 (5)	2.750 (2)	178 (7)
O6—H6*W*···O5	0.84 (2)	1.94 (2)	2.765 (2)	170 (5)
C2—H2···O6^{xiv}	0.95	2.53	3.230 (2)	131
C8—H8*B*···O6^{xiv}	0.98	2.48	3.383 (2)	152
C6—H6···O5^{xvi}	0.95	2.47	3.179 (2)	132

Symmetry codes: (i) $-x, -y, -z+2$; (ii) $x, y-1, z$; (iii) $x, y, z-1$; (iv) $-x+2, -y+1, -z+1$; (v) $-x+1, -y+1, -z+1$; (vi) $x, y, z+1$; (vii) $-x+1, -y+2, -z+1$; (viii) $-x+\frac{1}{2}, y+\frac{1}{2}, -z+\frac{1}{2}$; (ix) $-x+\frac{1}{2}, y-\frac{1}{2}, -z+\frac{1}{2}$; (x) $x, -y+1, z+\frac{1}{2}$; (xi) $-x, -y+2, -z+1$; (xii) $x+1, y, z$; (xiii) $-x, -y+1, -z+1$; (xiv) $-x+1, -y+1, -z$; (xv) $-x+1, -y, -z$; (xvi) $-x, -y+1, -z$.

(Etter *et al.*, 1990) (Fig. 3*a*). This strong intermolecular interaction arranges the molecules into a 2D sheet in the *ab* crystallographic plane. These sheets are connected by methyl and ring protons to adjacent carboxylate O atoms, forming weak C8—H8*C*···O1^{iii} and C2—H2···O2^{iii} interactions (Fig. 3*b*) in the *cb* plane. Short ring–ring interactions between parallel pyridine rings, with a distance of 3.4715 (16) Å, increase the stability of the lattice. The crystal contains alternating hydrophobic and hydrophilic layers repeated in the crystallographic *c* direction (Fig. 3*c*). Interatomic distances and angles of some selected secondary interactions are collected in Table 3.

3.3. Structural analysis of [Zn(A2)$_2$(H$_2$O)] (2)

The Zn^{II} crystal of A2, *i.e.* **2**, was colourless and block-shaped in the triclinic space group $P\overline{1}$ (the same as **1**). In **2**, however, the whole complex is in the asymmetric unit, not only half as in **1**, and the inversion centre is positioned between two adjacent molecules. The two ligands coordinate asymmetrically and this is manifested in different dihedral angles between the coordination plane and the pyridine ring planes. The first ligand lies almost in the coordination plane, as the angle between the O2/Zn1/O3 plane and the pyridine-ring plane is 1.88 (8)°, while for the second ligand, this angle is 22.95 (8)°. This also means that the two pyridine rings are closer to perpendicular than to planar geometry, and the angle between the two ring planes is 60.72 (11)° (see Table S1 in the supporting information). The two ligands coordinate in mutually *trans* positions, although the equatorial plane is highly distorted, resulting in an almost trigonal bipyramidal geometry (Fig. 4). The Zn^{II}—O(carboxylate) distances Zn1—O2 and Zn1—O12 are significantly shorter [1.9619 (17) and 1.9729 (17) Å, respectively] than the Zn^{II}—O(oxide) bonds Zn1—O3 and Zn1—O13 [2.0799 (17) and 2.0454 (17) Å, respectively; see Table 2]. At the same time, the Zn—O bond to the aqua ligand has almost the same length [2.004 (2) Å] as those to the O2 and O12 donor groups, so that the trigonal bipyramidal geometry is supported. The O2—Zn1—O4 angle is 123.57 (8)° and the O2—Zn1—O12 angle is 113.47 (7)°, which are also close to the angle of 120° expected for a trigonal bipyramidal complex. In order to decide whether the geometry of the coordination centre is trigonal bipyramidal or square pyramidal, the τ_5 (originally just τ) parameter was introduced by Addison *et al.* (1984). This parameter is calculated with the equation $\tau_5 = (\beta - \alpha)/60$, where $\beta > \alpha$ are the two largest valence angles of the coordination centre. When τ_5 is close to 0, the geometry is similar to square pyramidal, while if τ_5 is close to 1, the geometry is similar to trigonal bipyramidal. In **2**, the τ_5 value is 0.837, confirming the trigonal bipyramidal geometry. As a consequence of this conformation, the two ligands turn out of the equatorial plane so that the dihedral angle between the pyridine-ring planes of the two ligands is 60.72 (11)°.

In comparison, the Cu^{II} complex with the A2 ligand displays a square-pyramidal geometry with axial bonding of the neighbouring carboxylate O atom in a *syn–anti* coordination mode, resulting in a one-dimensional (1D) polymer chain (Fig. S2 in the supporting information; May *et al.*, 2019). The formation of 1D polymer chains was not unexpected because the methyl groups introduced into the pyridine ring inhibit the formation of a cyclic dimer similar to that obtained in the case of [Cu$_2$(A1)$_4$]·4H$_2$O (Fig. S1). Selected distances and angles measured in the coordination sphere of the Zn^{II} and Cu^{II} complexes with ligand A2 are collected in Table 2 and Table S2 in the supporting information, respectively.

In **2**, the complex molecules are arranged in 1D columns along the crystallographic *c* axis, organized by O4—H1O···O1^{iv} [graph-set descriptor $R_2^2(12)$ and O4—H1*W*···O3^{v} [$R_4^2(8)$] interactions (Fig. 5*a*) around an inversion centre placed in the middle of each ring of intermolecular interactions. There are inter-column C—H···O interactions between the methyl protons and carboxylate O atoms, *i.e.* C8—H8*C*···O12^{vii}, C8—H8*B*···O11^{vi}, C9—H9*B*···O12^{vii} and C9—H9*C*···O11^{vi} (Fig. 5*b*). Face-to-face π–π interactions, with a distance of 3.669 (12) Å, are present between the pyridine rings. The crystal contains alternating hydrophobic and hydrophilic layers repeated in the crystallographic *a* direction (Fig. 5*c*), with more distortion than in **1**.

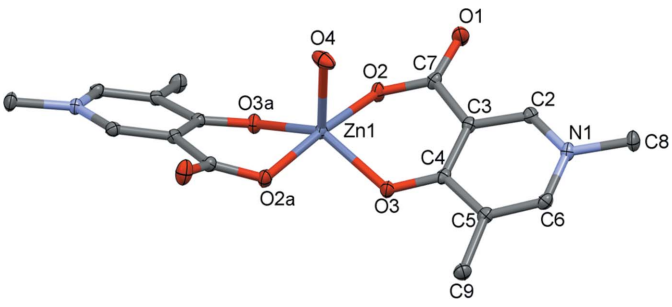

Figure 6
The molecular structure of $[Zn(A3)_2(H_2O)]\cdot 2H_2O$, **3**, with displacement ellipsoids drawn at the 50% probability level. H atoms and water molecules of crystallization have been omitted for clarity. For atom labels, suffix a = $-x, y, \frac{1}{2} - z$.

3.4. Structural analysis of $[Zn(A3)_2(H_2O)]\cdot 2H_2O$ (3)

The SXRD study shows that **3** crystallizes in the monoclinic space group *C*2/*c*. The asymmetric unit consists of half of the complex (half a metal ion with half of the axially coordinated water molecule, one A3 ligand and one water molecule of crystallization), as the Zn1—O4 bond lies on a twofold axis (Fig. 6). The dihedral angle between the planes generated by the coordinating atoms (O2/Zn1/O3) and pyridine ring is 28.26 (5)° for both ligands, and the angle between the two pyridine-ring planes is 41.32 (9)° (Table S1 in the supporting information). Zn1 is five-coordinated, exhibiting a geometry between square pyramidal and trigonal bipyramidal. The τ_5 parameter was calculated to be 0.592, which is less than in the case of **2**, but is still closer to trigonal bipyramidal geometry than to square pyramidal. No comparison is possible for the complex formed by A3 with Cu^{II} as the latter has not be crystallized thus far. The conformations of the two trigonal bipyramidal structures (**2** and **3**) differ considerably (Fig. S10 in the supporting information). The Zn—O2, Zn—O3 and Zn—O4 bond lengths are almost equal in this complex [1.9993 (10)–2.0282 (12) Å; Table 2], so that the water O atom has a similar binding strength to the ligand O-donor atoms. The two ligands are rotated out of the equatorial plane, but the angle between the two pyridine-ring planes is smaller [41.32 (9) Å] than in **2** [60.72 (11) Å]. Bond lengths and angles measured between the atoms of the coordination sphere are collected in Table 2.

There are similarities in the packing arrangements of complexes **2** and **3** (compare Fig. 6*b* with Fig. 7*b*), as the carboxylate O atoms bind to $>N^+—Me$ protons in both structures, *via* C8—H8*C*···O12^{vii} and C8—H8*B*···O11^{vi} hydrogen bonds in **2**, and C8—H8*B*···O2^{x} and C8—H8*C*···O1^{v} hydrogen bonds in **3** (Table 3). While the protons of the axially coordinated water molecule are connected directly to the carboxylate O atom of the neighbouring com-

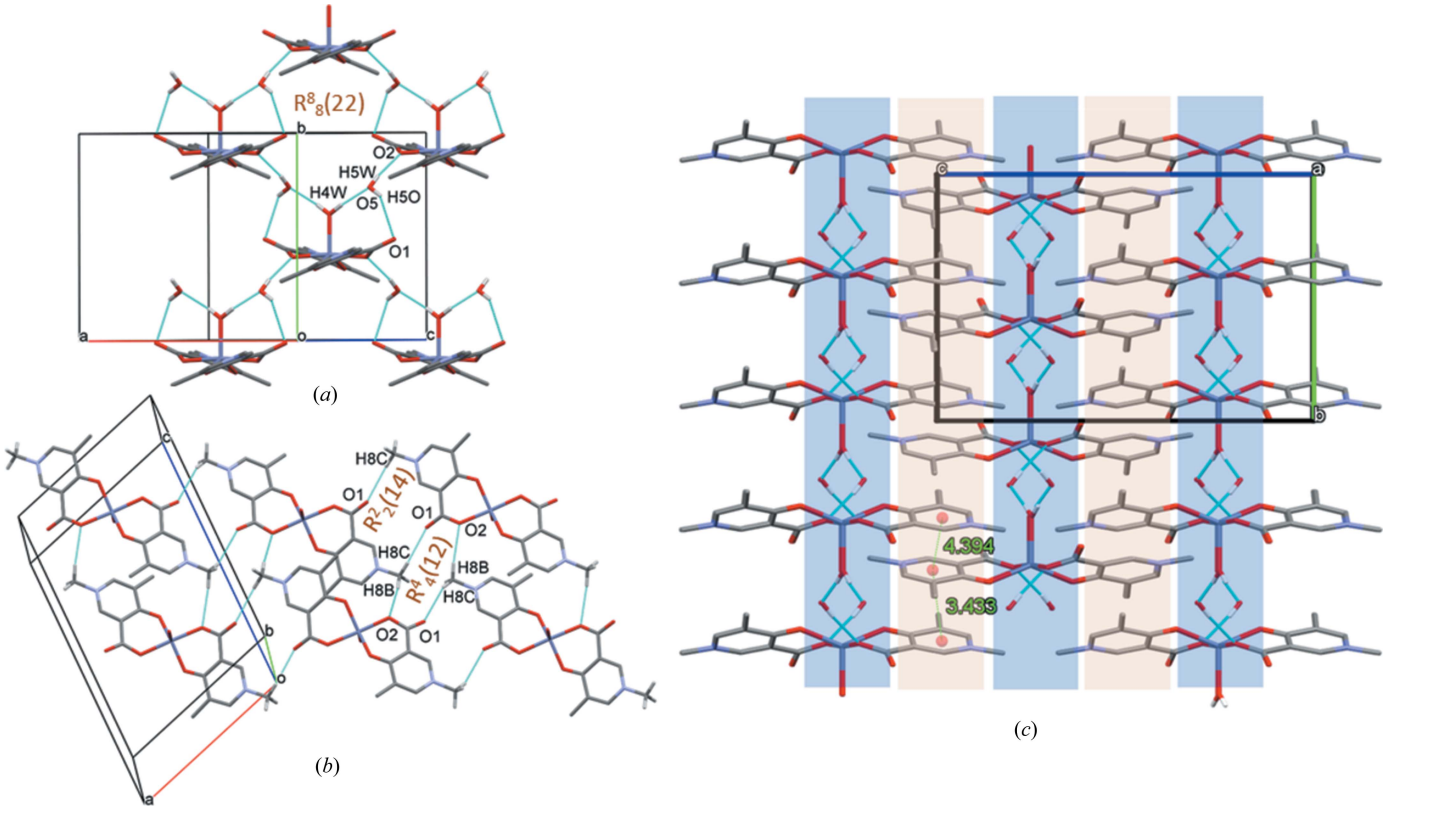

Figure 7
The packing arrangements in **3**, showing the main (*a*) O—H···O and (*b*) C—H···O intermolecular interactions, and (*c*) the alternating hydrophilic (blue) and hydrophobic (grey) layers, viewed from the crystallographic *a* direction. Ring–ring distances are shown in Å.

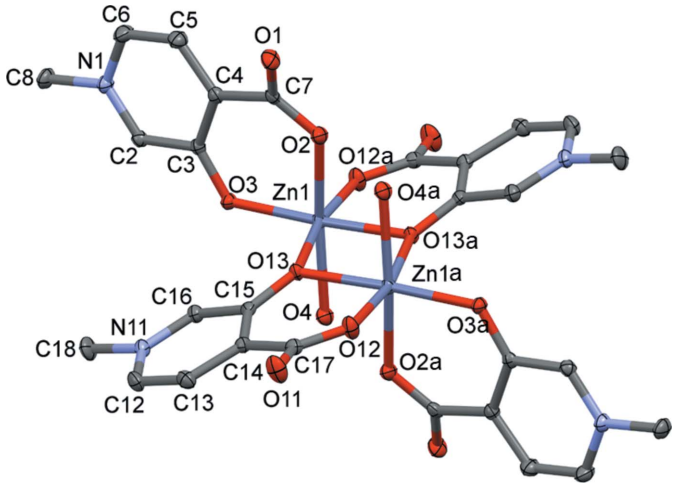

Figure 8
The molecular structure of $[Zn_2(B1)_4(H_2O)_2]\cdot 4H_2O$, **4**, with displacement ellipsoids drawn at the 50% probability level. H atoms and water molecules of crystallization have been omitted for clarity. For atom labels, suffix a = $-x, 2-y, 1-z$.

plex in the complexes of A1 and A2, in the complex with A3, the water protons and the neighbouring carboxylate O atoms are connected through a water molecule of crystallization as a bridge between the complex molecules below and above each other (Fig. 7*a*). The main hydrogen-bond interactions, O4—H4*W*···O5^{viii}, O5—H5O···O1^{ix} and O5—H5*W*···O2, connect four complex molecules in a ring by the graph set $R_8^8(22)$, organized by twofold and twofold screw axes, and intersected by a glide plane but lacking inversion symmetry. These are further connected, forming a 2D sheet in the crystallographic *ab* plane; data are shown in Table 3. Carboxylate O atoms are connected with the >N$^+$—Me group protons of an adjacent complex in a neighbouring plane by C8—H8*B*···O2^x, forming an $R_3^2(14)$ ring, and by C8—H8*C*···O1^v, forming an $R_4^4(12)$ ring (Fig. 7*b*). The shortest pyridine–pyridine ring distance measured between the centres of gravity of two rings is 3.4325 (9) Å. The alternating hydrophobic and hydrophilic sheets can be recognized even in this structure (Fig. 7*c*).

3.5. Structural analysis of $[Zn_2(B1)_4.(H_2O)_2]\cdot 4H_2O$ (4)

In ligand B1, the positions of the oxide and carboxylate groups on the pyridine ring are interchanged, which alters significantly the electron distribution of the O-donor atoms. In the case of the Cu^{II} complex, *i.e.* $[Cu(B1)_2(H_2O)]\cdot 3H_2O$, this results in the coordination of the two ligands in a *cis* arrangement (Fig. S3 in the supporting information) instead of the *trans* arrangement that was observed for the Zn^{II} and Cu^{II} complexes of A1. The Cu^{II} complex is five-coordinated in a square-pyramidal geometry, with a water molecule coordi-

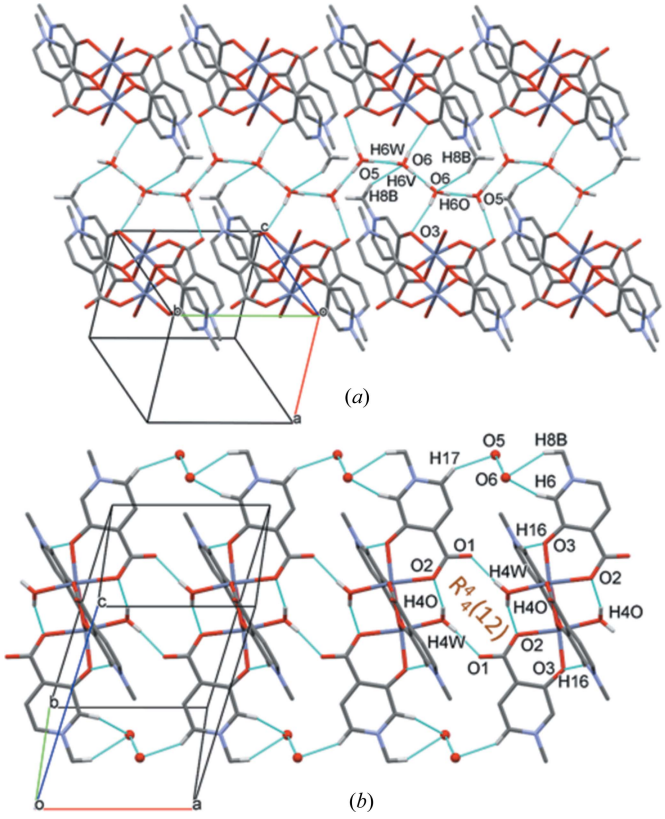

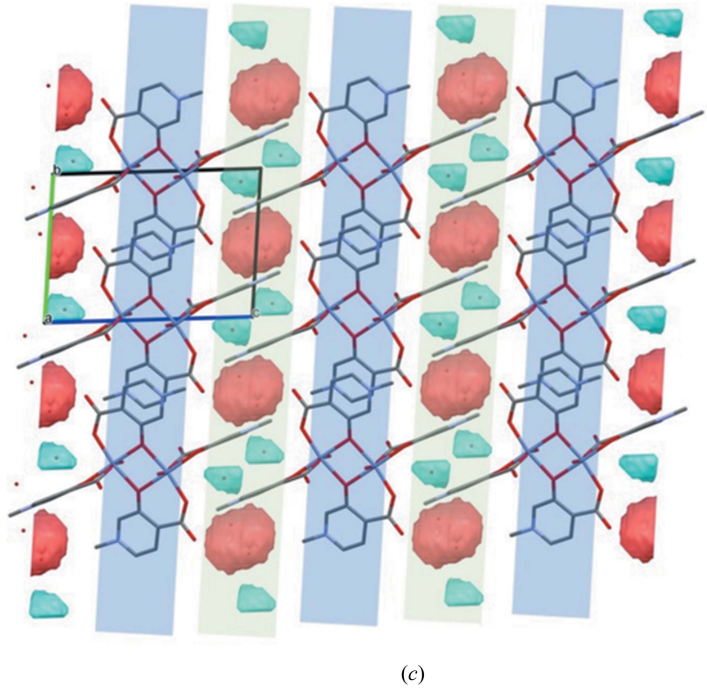

Figure 9
The packing arrangements in **4**, showing the main (*a*) O—H···O and (*b*) C—H···O intermolecular interactions, and (*c*) layers, viewed from the crystallographic *a* direction. Hydrophobic layers (blue) found in **1**–**3** alternate with layers (green) which contain water molecules of crystallization (red and green voids) together with the aromatic rings.

nated in the axial position. In the case of Zn^{II}, however, the complex of B1 resulted in a dimeric structure. This was a surprising result as the formation of dimeric (dinuclear complex) of HPCs with Zn^{II} has not been reported to occur in the solution state (Sija *et al.*, 2014). The dimeric complex crystallizes in the triclinic space group $P\overline{1}$ and has two coordinated water molecules and four additional water molecules of crystallization. One Zn^{2+} ion, two ligands, one coordinated axially, and two solvent water molecules form the asymmetric unit (Fig. 8), and the other half of the dimeric complex is formed repeating this part through an inversion centre positioned between the two Zn1 ions. Shorter Zn—O bond lengths are found in the six-membered chelate rings (Zn1—O3, Zn1—O2, Zn1—O12 and Zn1—O13), while longer bond lengths are found for the water Zn1—O4 and the bridging oxide Zn1—O13 bonds (Table 2).

The packing of the molecules in **4** is dominated by O—H···O hydrogen bonds with the participation of the axially coordinated water protons and the water molecules of crystallization. The intramolecular O4—H4O···O2^{xi} interaction between the axially coordinated water and the carboxylate O atom stabilizes the binuclear complex, while the other coordinated water proton connects two dimeric units together [graph set $R_4^4(12)$], thus forming a chain of complex molecules in the crystallographic *a* direction. The O5 and O6 water molecules are located in channels in the crystallographic *b* direction and are involved in hydrogen bonds as hydrogen-bond donors in three different directions. They are connected to the acceptor O3 and O11 atoms of the ligands, respectively. Furthermore, the direction of the hydrogen bonds alternates in the columns formed by the water molecules of crystallization; thus, the protons appear between the two O atoms connected alternately to one of them and so both protons could be found in difference Fourier maps. These protons (H5*V*/H5*W* and H6*V*/H6*W*) were refined with an occupancy of 0.5. The water molecules of crystallization take part in further C—H···O interactions as acceptors with the >N$^+$—Me protons of adjacent ligands (Fig. 9). Selected hydrogen-bond parameters of **4** are collected in Table 3.

The alternating packing arrangement observed in the crystal structures of **1**–**3** is modified in **4** as a result of the exchange of the positions of the carboxylate and oxide groups (Fig. 9*c*). The former hydrophobic layer is completed, with the zigzag chain of connected water molecules of crystallization separating neighbouring complexes.

3.6. Comparison of the supramolecular interactions by Hirshfeld surface analysis

The Hirshfeld surfaces of the investigated molecules in **1**–**4** were calculated in order to compare the supramolecular interactions (Fig. S11–S13 in the supporting information). The relative contributions of the main intermolecular contacts O···H/H···O, H···H, C···H/H···C and C···C are shown in Fig. 10. The ratio of the O···H/H···O contacts is the highest in **1**, presumably because there are two axial water molecules in this complex, while the others have only one. There is one more methyl group in ligands A2 and A3 compared to A1, which should increase the H···H contacts in the crystal, and this can be seen in the case of **3**. However, in **2**, the relative contribution of H···H contacts to the Hirshfeld surfaces has decreased. At the same time, the percentage of C···H contacts increases in **2** compared to **1**, which means that neighbouring ligands are packed in such a way that the methyl protons are closer to the C atoms of the pyridine ring than to each other. The largest contribution of the C···C contact to the Hirshfeld surface can be seen in **3**, which also has the shortest ring–ring distance. In **4**, the Hirshfeld surface was calculated for the dimer unit. Despite the presence of the four water molecules of crystallization, the percentage of O···H/H···O contacts is lowest here, likely because the water molecules are mainly connected to each other in a channel in the crystal lattice.

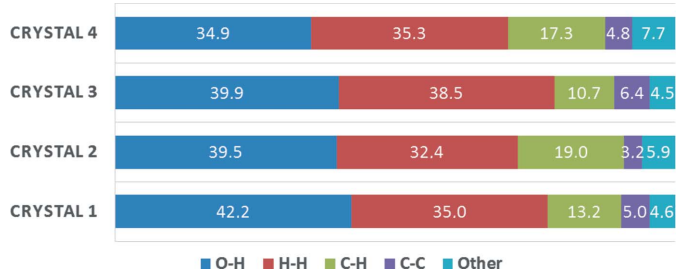

Figure 10
The relative contributions (%) of the various intermolecular contacts to the Hirshfeld surface area in **1**–**4** (for further details, see Fig. S11 in the supporting information).

3.7. Comparison of the coordination spheres in 1–4

Two of the investigated bis-ligand Zn^{II} complexes contain a six-coordinated metal ion (with ligand A1 and B1) and the other two complexes exhibit five-coordination (with ligands A2 and A3). Although the two donor groups of the ligands could have resulted in a tetrahedral geometry with four-coordination, the coordination spheres were completed in all cases by one or two water molecules, resulting in five- or six-coordination geometries instead.

The coordination spheres in the investigated crystals are compared in Fig. 11. A highly symmetrical octahedral geometry with two axial water molecules and an inversion centre coinciding with the Zn^{II} position was detected in the complex of ligand A1 (crystal **1**) (Fig. 11*a*). A less symmetrical octahedron is seen in the dimer of B1 (crystal **4**), with one axial water molecule and an equatorial coordination of the neighbouring ligand O13*a* atom (Fig. 11*b*). The bis-ligand Zn^{II} complexes of A2 and A3 display a five-coordinated trigonal bipyramidal geometry in **2** and **3**, with the coordination of one water molecule (Figs. 11*c* and 11*d*). The differences between the structures of **2** and **3** are as follows: (i) in **3**, a twofold rotation axes coincides with the Zn1—O4 bond, while this symmetry element is missing in **2**, and (ii) in **2**, the ligand carboxylate O atoms (O2 and O12) coordinate equatorially to the metal ion, while it is the oxide O atom (O3) in the case of **3**. The calculated τ_5 values (0.837 and 0597, respectively) show

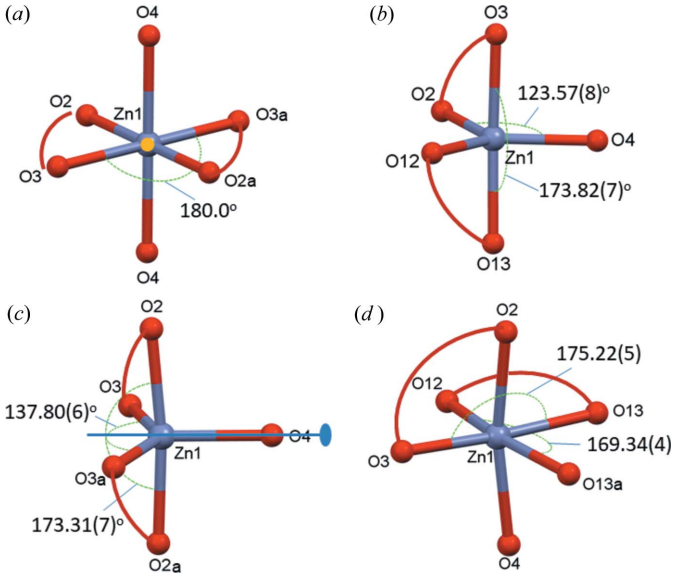

Figure 11
Comparison of the coordination spheres of Zn^{II} in (*a*) **1** (for atom labels, suffix $a = 1 - x, y, 2 - z$), (*b*) **2**, (*c*) **3** (for atom labels, suffix $a = -x, y, \frac{1}{2} - z$) and (*d*) **4** (for atom labels, suffix $a = -x, 2 - y, 1 - z$). The largest valence angles are shown.

a more symmetrical trigonal bipyramidal geometry for **2** than for **3**. Fig. S10 (see in the supporting information) shows an overlay of the crystal structures of **2** and **3**.

In order to investigate the occurrences of the different geometries among five-coordinated Zn^{II} complexes, conformational data were collected from the CSD. Up until early 2020, 3176 structures of solely oxygen-coordinated Zn^{II} complexes had been deposited with the coordination of exactly four O-atom donors (4O-coordination), 1284 with 5O-coordination and 2906 with 6O-coordination. This distribution shows that Zn^{II} has a preference to form tetragonal and hexagonal complexes, although five-coordination is also seen,

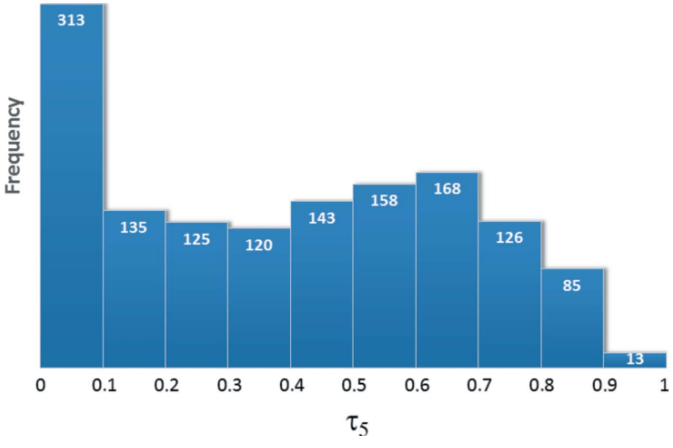

Figure 12
Histogram showing the τ_5 values for 5O-coordinated Zn^{II} complexes deposited in the CSD.

but with slightly fewer occurrences. In the case of five-coordination, the 1284 entries contained 1629 Zn^{II} complexes with 1386 different structures left after filtering out entries with identical structures. The τ_5 value for each was calculated to establish the distribution of the occurrences of square-pyramidal and trigonal bipyramidal structures among the 5O-coordinated Zn^{II} complexes. The histogram obtained from the distribution of the occurrences of the τ_5 values is shown in Fig. 12. The highest occurrence can be observed with low τ_5 values (τ_5 = 0–0.1), which belongs to square-pyramidal geometry. The higher τ_5 values show a more even distribution until $\tau_5 < 0.8$, with a maximum around 0.65. With τ_5 above 0.8, the number of occurrences is significantly decreased, so that only a few structures have closely symmetrical trigonal bipyramidal geometry. It can be deduced that **2** and **3** are atypical structures, and the τ_5 value of 0.837 in the case of ligand A2 corresponds to a rather unusual Zn^{II} complex geometry. As a comparison, τ_5 values were also calculated for the 5O-coordinated Cu^{II} complexes, and it was found that the incidence of trigonal bipyramid geometry here is even lower, as 97% ($\tau_5 < 0.5$) of the structures have square-pyramidal geometry (Fig. S14 in the supporting information). In our analogous Cu^{II} complexes of ligands A1, A2 and B1, only square-pyramidal geometry was found.

The preference to form bis-ligand complexes in a *trans* orientation remained for ligands A1, confirming that this arrangement depends on the electronic distribution of the ligands and not on the crystal packing. In the case of Cu^{II}, the geometry is primarily determined by the crystal field, resulting in square-pyramidal geometry being energetically more favourable.

The splitting of the *d*-orbitals, as a consequence of the Jahn–Teller effect, appears to be the greatest driving force in the design of the complexes, resulting in a less tight fit of the Cu^{II} complexes; the gaps between the complexes are then filled with water molecules of crystallization (three or four water molecules per complex; see Figs. S15–S17 in the supporting information). It can be concluded from the coordination analysis that the coordination geometry of the Zn^{II} complexes is more flexible, and the coordination sphere accommodates better to the neighbouring complexes to form a tight fit in the crystal lattice. This is reflected in the water content of the relevant Cu^{II} and Zn^{II} crystals. While in $[Cu_2(A1)_4]\cdot 4H_2O$ and $\{[Cu(A2)_2]\cdot 3H_2O\}_n$, the water of crystallization is 11.5 and 11.4% of the unit-cell volume, respectively (Figs. S15 and S16 in the supporting information), the Zn^{II} analogues **1** and **2** do not contain water of crystallization. In the case of B1, the formed dimer fixes the geometry around the Zn^{II} ions and the water content is similar to and as high as in the Cu^{II} analogue (7.2 and 5.6%, respectively; see Figs. S17 and S18 in the supporting information).

We note that the complex crystals have been isolated from aqueous solutions containing a twofold ligand excess, and other ligand-to-metal concentration ratios or solvents have not been tested, so that the formation of other crystal forms or coordination geometries under different conditions cannot be excluded. Based on our previous solution speciation study

(Sija *et al.*, 2014), we may expect that by dissolving any of the investigated [ZnL_2] crystals in aqueous solution, it would partially dissociate and a mixture of mono- and bis-ligand complexes would be obtained. The formation of square-pyramidal or octahedral Zn^{II} complexes is more likely in solution than trigonal bipyramidal complexes, which are stabilized by secondary interactions in the crystals, and the formation of the *cis* isomer cannot be excluded either. Solution equilibrium studies did not show dimer formation with Zn^{II}, but with Cu^{II}, dimer formation could be detected in the frozen solution by electron spin resonance (ESR) spectroscopy (May *et al.*, 2019).

4. Conclusions

The single-crystal structures of bis-ligand Zn^{II} complexes of four *O*,*O*′-donor hydroxypyridinecarboxylate ligands have been determined. Despite their identical bidentate coordination modes, various geometries have been obtained. The most common geometry in the case of Zn^{II} with a d^{10} electronic configuration would be tetragonal or octahedral, based on crystal field theory. Here, after crystallization water solution at pH $\sim$ 7, the formation of one octahedral complex with two axially coordinated water molecules, [Zn(A1)$_2$(H_2O)$_2$] (**1**), two complexes with one axial water coordination and trigonal bipyramidal geometry, [Zn(A2)$_2$(H_2O)] (**2**) and [Zn(A3)$_2$-(H_2O)]·2H_2O (**3**), and a dimeric structure with an oxide O-atom bridge, [Zn_2(B1)$_4$(H_2O)$_2$]·4H_2O (**4**), was established. The structural variety is probably not only due to the electronic differences between the ligands, but also to the adaptation of the coordination geometry to the close crystal packing to maximize the attractive interaction between ligands and to create a tight fit in the crystal. There is a common packing pattern containing alternating hydrophilic and hydrophobic layers irrespective of the substitution, coordination and space group. This pattern can be broken only by the exchange of the positions of the oxide and carboxylate groups.

Comparing the Zn^{II} complexes with the Cu^{II} analogues, we conclude that, due to the different number of electrons (d^9 for Cu^{II}), square-pyramidal geometry with a longer axial bond is preferred in the bis-ligand copper complexes. In these complexes of A1 and A2, the axial donor atom is a neighbouring carboxylate O atom, while in B1 it is a water O atom. In these Cu^{II} analogues, a large number of molecules of water of crystallization was found, so that the geometry of the complex appears to be strongly fixed by regulation of crystal field and the voids between the molecules are filled with solvent molecules. In this case, the packing of the complexes does not induce any effect on the geometry of the complex, in contrast to that observed for zinc complexes. However, we cannot exclude the formation of other possible geometries of these complexes in other crystal forms by the use of different crystallization conditions and solvents.

A comprehensive CSD study of Zn complexes coordinated with a different number of O atoms has been performed. According to the CSD, we conclude that trigonal bipyramidal geometry is rather uncommon for 5O-coordinated zinc complexes, and with $\tau_5 > 0.8$, the geometry obtained in **2** is quite rare.

Funding information

The following funding is acknowledged: FWO-MTA (contract No. PROJEKT2017-16); Nemzeti Kutatási Fejlesztési és Innovációs Hivatal, Hungarian Scientific Research Fund (contract Nos. K124544, KH129588 and PD128504 to TH); Magyar Tudományos Akadémia, J. Bolyai Research Scholarship (scholarship No. BO/00109/17 to NVM; scholarship No. BO/00146/17 to TH).

References

Addison, A. W., Rao, N. T., Reedijk, J., van Rijn, J. & Verschoor, G. C. (1984). *J. Chem. Soc. Dalton Trans.* pp. 1349–1356.
Biradha, K., Su, C.-Y. & Vittal, J. J. (2011). *Cryst. Growth Des.* **11**, 875–886.
Burla, M. C., Caliandro, R., Carrozzini, B., Cascarano, G. L., Cuocci, C., Giacovazzo, C., Mallamo, M., Mazzone, A. & Polidori, G. (2015). *J. Appl. Cryst.* **48**, 306–309.
Clarke, E. T. & Martell, A. E. (1992). *Inorg. Chim. Acta*, **57**, 191.
Crisponi, G., Dean, A., Di Marco, V. B., Lachowicz, J. I., Nurchi, V. M., Remelli, M. & Tapparo, A. (2013). *Anal. Bioanal. Chem.* **405**, 585–601.
Dean, A., Ferlin, M. G., Brun, P., Castagliuolo, I., Yokel, R. A., Badocco, D., Pastore, P., Venzo, A., Bombi, G. G. & Di Marco, V. B. (2009). *Dalton Trans.* pp. 1815–1824.
Dean, A., Ferlin, M. G., Carta, D., Jakusch, T., Kiss, T., Faccioli, F. F., Parrasia, S., Marton, D., Venzo, A. & Di Marco, V. (2018). *J. Solution Chem.* **47**, 92–106.
Dean, A., Ferlin, M. G., Cvijovic, M., Djurdjevic, P., Dotto, F., Badocco, D., Pastore, P., Venzo, A. & Di Marco, V. B. (2014). *Polyhedron*, **67**, 520–528.
Desiraju, G. R. (2003). *J. Mol. Struct.* **656**, 5–15.
Di Marco, V. B., Dean, A., Ferlin, M. G., Yokel, R. A., Li, H., Venzo, A. & Bombi, G. G. (2006). *Eur. J. Inorg. Chem.* **2006**, 1284–1293.
Di Marco, V. B., Yokel, R. A., Ferlin, M. G., Tapparo, A. & Bombi, G. G. (2002). *Eur. J. Inorg. Chem.* **2002**, 2648–2655.
Etter, M. C., MacDonald, J. C. & Bernstein, J. (1990). *Acta Cryst.* B**46**, 256–262.
Farrugia, L. J. (2012). *J. Appl. Cryst.* **45**, 849–854.
Groom, C. R., Bruno, I. J., Lightfoot, M. P. & Ward, S. C. (2016). *Acta Cryst.* B**72**, 171–179.
Higashi, T. (2002). *NUMABS*. Rigaku Corporation, Tokyo, Japan.
Higashi, T. (2011). *NUMABS*. Rigaku Corporation, Tokyo, Japan.
Li, J. (2019). *Mediterr. J. Hematol. Infect. Dis.* **11**, e2019036.
Macrae, C. F., Sovago, I., Cottrell, S. J., Galek, P. T. A., McCabe, P., Pidcock, E., Platings, M., Shields, G. P., Stevens, J. S., Towler, M. & Wood, P. A. (2020). *J. Appl. Cryst.* **53**, 226–235.
May, N. V., Gál, G. T., Szentendrei, Z., Korecz, L., May, Z., Ferlin, M. G., Dean, A., Bombicz, P. & Di Marco, V. B. (2019). *New J. Chem.* **43**, 10699–10710.
McKinnon, J. J., Spackman, M. A. & Mitchell, A. S. (2004). *Acta Cryst.* B**60**, 627–668.
Pashadilis, I. & Kontoghiorghes, G. J. (2001). *Arzneim. Forsch. Drug. Res.* **51**, 998–1003.
Rigaku (2015). *RAPID-AUTO*. Rigaku Corporation, Tokyo, Japan.
Rigaku/MSC Inc. (2008). *CrystalClear*. Rigaku/MSC Inc., The Woodlands, Texas, USA.
Sheldrick, G. M. (2015*a*). *Acta Cryst.* A**71**, 3–8.
Sheldrick, G. M. (2015*b*). *Acta Cryst.* C**71**, 3–8.

Sija, É., Nagy, N. V., Gandin, V., Marzano, C., Jakusch, T., Dean, A., Di Marco, V. B. & Kiss, T. (2014). *Polyhedron*, **67**, 481–489.
Spackman, M. A. & Jayatilaka, D. (2009). *CrystEngComm*, **11**, 19–32.
Spackman, M. A. & McKinnon, J. J. (2002). *CrystEngComm*, **4**, 378–392.
Spek, A. L. (2020). *Acta Cryst.* E**76**, 1–11.
Turner, M. J., McKinnon, J. J., Wolff, S. K., Grimwood, D. J., Spackman, P. R., Jayatilaka, D. & Spackman, M. A. (2017). *CrystalExplorer17*. University of Western Australia. https://crystalexplorer.scb.uwa.edu.au.
Westrip, S. P. (2010). *J. Appl. Cryst.* **43**, 920–925.